Journal of
Materials Chemistry B

Materials for biology and medicine

Accepted Manuscript

This article can be cited before page numbers have been issued, to do this please use: L. Ma, M. Liu, X. Liu, W. Sun, Z. Lu, Y. Gao and L. He, *J. Mater. Chem. B*, 2020, DOI: 10.1039/D0TB00321B.

ROYAL SOCIETY OF CHEMISTRY

rsc.li/materials-b

View Article Online
DOI: 10.1039/D0TB00321B

ARTICLE

Macrocyclic Polyamine [12]aneN$_3$ Modified Triphenylamine-Pyrazine Derivatives as Efficient Non-viral Gene Vectors with AIE and Two-photon Imaging Properties

Received 00th January 20xx,

Accepted 00th January 20xx

DOI: 10.1039/x0xx00000x

Le-Le Ma,[a] Ming-Xuan Liu,[a] Xu-Ying Liu,[a] Wan Sun,[a] Zhong-Lin Lu,*[,a] Yong-Guang Gao,*[,b] and Lan He *[,c]

With the aim to develop a novel multifunctional gene delivery system that may overcome the common barriers of gene transfection, the near-infrared fluorescent triphenylamine-pyrazine was modified with DNA condensing moieties triazole-[12]aneN$_3$ through the different length alkyl ester linkage to afford three new non-viral gene vectors, **TDM-A/B/C**. All compounds showed prominent solvatochromic fluorescent (stocks shift up to 383 nm), two-photon absorption properties (σ2P to 101 GM), and exhibited strong aggregation-induced emission (AIE) property. Gel electrophoresis demonstrated that plasmid DNA were completely condensed at a concentration of 10 μM (**TDM-A**), 14 μM (**TDM-B**) and 16 μM (**TDM-C**), and released under esterase and acidic environment. SEM demonstrated the three compounds were able to be self-assembled and co-aggregated with DNA to form regular nanoparticles. Experiments demonstrated that **TDM-A/B/C** were able to integrate with DNA through electrostatic interactions and supramolecular stacking, and short alkyl linkage favored to the strong interaction with DNA. Among the three compounds, **TDM-B** showed the best luciferase and GFP transfection activities in the presence of DOPE, which were 156% and 310% higher than those of Lipo2000. The transfection process of DNA was clearly traced through one- and two-photon fluorescence microscopic imaging. Cellular uptake inhibition assay indicated that the DNA complex entered the cell mainly via clathrin-independent endocytosis. Furthermore, the *in vivo* transfection experiments of **TDM-B**/DOPE were successfully implemented in zebrafish embryos, and the GFP gene expression level was superior to Lipo2000 (200%). Finally, this study clearly unraveled that the length of the alkyl linkage affected the DNA condensation and transfection activity which can be served as a base for future rational design of non-viral gene vectors.

1. Introduction

Gene therapy is full of promise in treating human diseases, like cancers and gene defects， which is strongly determined by gene delivery systems.[1-3] A desirable vector can promote the gene cargo delivering into target cells as well as keeping the packaged therapeutic genes from the biodegradation, and also the efficient release of the carried genes in cytoplasm or nucleus.[4,5] Engineered viruses were first used in gene delivery systems for the satisfactory results revealed in several initial clinical trials.[6,7] However, their intrinsic immunogenicity, notable toxicity, and mutagenic effects hindered their wide applications.[8-11] For this reason, non-viral vectors have received increased attention because they can be tailored and synthesized to satisfy different needs of gene delivery.[12] During the past decades, various types of non-viral vectors have been extensively investigated such as lipids, polymers, dendrimers and inorganic nanoparticles, and greatly progress has also been achieved.[13,14] Nevertheless, the low transfection efficiency of non-viral vectors remains a critical issue, the design and synthesis of non-viral vectors are still highly needed for the efficient transfection.[15-17]

Moreover, it is also very important for vectors to effectively elucidate DNA cellular uptake mechanisms during the delivery process, including internalization pathway, and endosomal release. To track gene delivery processes, coumarin, naphthamide, tetraphenylethene and other fluorophores have been incorporated in various non-viral gene vectors.[18-21] However, those commonly used fluorophores still encounter lots of obstacles for their poor sensitivity and high background interference. At present, far-red and near-infrared (NIR) fluorescent materials not only possess the characteristics of specific targeting capability but also have aggregation-induced emission (AIE) and strong two-photon absorption are much-sought-after for therapeutic and bioimaging applications, because of their high resolution and deep tissue penetration.[22-24] Accordingly, it is of the greatest interest to design novel vectors with the property of far-red and NIR emission, strong two-photon absorption and therapeutic effect. **DCDPP-2TPA**

[a] a Key Laboratory of Radiopharmaceutics, Ministry of Education; College of Chemistry, Beijing Normal University, Beijing 100875, P. R. China.
[b] b Lab for Bone Metabolism, Key Lab for Space Biosciences and Biotechnology, School of Life Sciences, Northwestern Polytechnical University, Xi'an, Shaanxi, 710072, China.
[c] c China National Institute for Food and Drug Control, Institute of Chemical Drug Control, TianTanXiLi 2, Beijing, 100050, China.

*Corresponding authors: luzl@bnu.edu.cn (Zhong-Lin Lu), helan1961@aliyun.com (Lan He) gaoyongguang@nwpu.edu.cn (Yong-Guang Gao)

Electronic Supplementary Information (ESI) available: [details of any supplementary information available should be included here]. See DOI: 10.1039/x0xx00000x

(Scheme **2**) is a type of aggregation-induced emission luminogen (AIEgen) with deep-red emissive, which were utilized as contrast agents for intravital imaging of mouse cerebral vasculature without craniotomy and skull-thinning.[25] Structurally, the rational design of gene vectors base on the understanding of their structure −property relationship. To promote the transfection efficiency, one of the most common methods is to modify different domains of the vectors, like hydrophilic domains, linker domains and hydrophobic domains.[26-29] Among the modifications of these domains, the hydrophobic modification as an effective and straightforward way has been established to promote endosomal escape and improve gene transfection.[30,31] However, the current hydrophobic modification studies were aimed at changing the length and number of aliphatic chains, and the effect of linker domains on the transfection is still rarely been reported.

Taking into account of the above considerations, we recently designed three novel non-viral gene vectors base on **DCDPP-2TPA** with different molecular structures via the esterification procedure and subsequent linker-chain functionalization using click chemistry, and their structure-property relationships toward gene delivery were systematic explored. Particularly, the strategy for exploiting ester bond break by hydrolysis to release DNA provides a promising approach for efficient transfection efficiency (Scheme 1). Through fluorescence spectroscopy, agarose gel electrophoresis (AGE), dynamic laser scattering (DLS), and scanning electronic microscopy (SEM) techniques, the relationships between the linkage length of the three derivatives and their ability toward DNA sensing, condensation, delivery, and transfection were studied in detail. The three vectors could efficiently deliver plasmid DNAs (pGL-3 and pEGFP-N1 reporter genes) into three type cells for genetic expression, and EGFP gene was even successfully transfected *in vivo* by **TDM-C**. The DNA delivery process were traced clearly through one- and two-photon fluorescence microscopic imaging.

2. Materials and methods

2.1. Materials

Unless otherwise specified, all the chemicals and analytical pure solvents were purchased from Energy Chemica (Shanghai, China), and used without further purification. Anhydrous ethanol, methanol, tetrahydrofuran (THF), dichloromethane (DCM) and N,N-dimethyl formamide (DMF) were dried and purified under nitrogen by using standard methods and were distilled immediately before use. Goldview II, 3-(4,5-dimethylthiazol-2-yl)-2,5-diphenyl tetrazoliumbromide (MTT), electrophoresis grade agarose, 6× loading buffer (30 mM EDTA, 40% glycerol, 0.03% xylene cyanol FF, and 0.05% bromophenol blue), ethidium bromide (EtBr), ctDNA (calfthymus DNA), pUC18 (plasmid DNA), Hochest 33342, micro BCA protein assay kit and luciferase assay kit were purchased from Solarbio Company (Beijing, China). DOPE (Dioleoylphosphatidyl ethanolamine) was from Santa Cruz Biotechnology (USA). Lipofectamine 2000™ was from Invitrogen (Life technologies, Mauricio Minotta, USA). Ultrapure milli-Q water (18.25 MΩ) was used in critical micelle concentration (CMC) and dynamic light scattering (DLS) tests. Tris-HCl buffer (pH 7.4) was used to conduct fluorescent titrations, gel electrophoresis at room

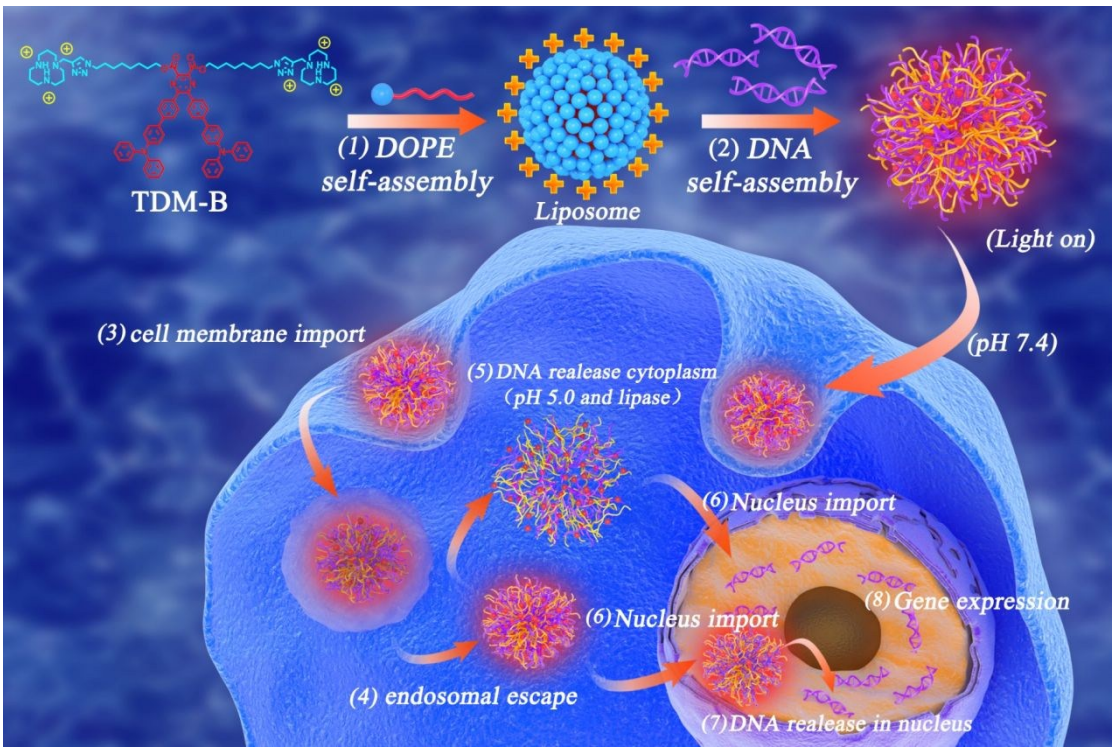

Scheme 1 Schematic illustration of the preparation and Characterization of liposome (TDM-B/DOPE) for Gene Delivery and transfection. (1) Self-assembly with DOPE. (2) DNA condensation (pH 7.4). (3) Cellular uptake via Endocytosis. (4) Endosomal escape in cytoplasm. (5) Control of ester bond cleavage and DNA release by lipase and pH 5.0. (6) Nucleus importation of DNA and DNA complex. (7) DNA release in nucleus. (8) Gene expression.

temperature. 6-carboxy-fluorescein FAM-labeled double-stranded oligomer 5'-GGTCGGAGTCAACGGATTTGGTCG-3', (FAM-DNA) and pGL-3 DNA were purchased from Ruibiotech Co., Ltd. (Beijing, China). Plasmid pEGFP-N1 was purchased from Clontech (Palo Alto, CA, USA).

The concentrations of ctDNA were determined by recording absorptions at 260 nm and applying Lambert–Beer's Law (molar absorption coefficient ε = 6600 M^{-1} cm^{-1}). ^{1}H and ^{13}C NMR spectra were obtained on a BrukerAvance III 400 MHz spectrometer at 25 ºC using $CDCl_3$ and DMSO-d_6 as solvents and calibrated using tetramethylsilane (TMS) as an internal reference. HRMS (High resolution mass spectra) were obtained on a Waters LCT Premier XE spectrometer (USA). Agarose electrophoresis was performed using a BG-subMIDI sub marine system (BayGene Biotech Company Limited, Beijing, China) and the electrophoresis images were obtained on a UVP EC3 visible imaging system (USA) using 254 nm UV light for visualization. The average particle sizes and zeta potentials of lipoplexes/DNA complex were detected by dynamic light scattering (DLS) on a Brookhaven Zeta Plus Partical Size and Zeta Potential Analyzer (USA). Fluorescence quantum yield was measured with an Absolute PL Quantum Yield Spectrometer QY C11347-11. Flow cytometry assays were performed on a CytoFLEX (Beckman-coulter, USA). Scanning electron microscopy (SEM) images were obtained with a Hitachi S-4800 (Japan) instrument. Fluorescence spectra were determined on a Hitachi F-4600 spectrophotometer. Absorption spectra were determined on a Shimadzu UV-1601PC UV-Visible spectrophotometer. Confocal fluorescence imaging was performed with Nikon A1R MP multiphoton microscopy with a 60×oil-immersion objective lens. Two-photon excitation fluorescence cross section was measured by two-photon excitation fluorescence method using rhodamine B as a reference. All the solutions were measured in a 3.5 mL (10 × 10 mm), 100 and 50 μL quartz cuvettes.

2.2. Fluorescence Measurements

Stock solutions (1 mM) of **TDM-A/B/C** were prepared in deionized Milli-Q water (18.25 MΩ). Stock solutions were diluted to certain volumes in volumetric flasks with appropriate aliquots and deionized Milli-Q water, and Tris-HCl buffer, and solutions of different concentrations were obtained. The DNA fluorescence titrations were performed using race-volume (100 or 50 μL) quartz cuvettes. After vortex mixed, all the samples allowed to rest for 6 - 10 min before testing.

2.3. Cell-uptake of liposome

The cellular uptakes of FAM-DNA (9 μg/mL) condensates were observed by fluorescence microscopy. Hela cells were cultured in DMEM medium supplemented with 10% FBS in a humid atmosphere containing 5% CO_2 at 37 °C. The cells were seeded in Glass Bottom Cell Culture Dishes at 1000 cells per dish and cultured for 24 h. After washing three times with DMEM, the cells were treated with freshly prepared compounds condensed FAM-DNA and the controls (500 μL) of DMEM. The Hochest 33342 (5 μg/mL) was also added to the cells for nuclear staining at 37 ºC for 15 min. Finally, the cells were washed for 5 times with PBS buffer, observed using a confocal laser scanning microscope with a 40× objective and DAPI filter for Hoechst 33342 (blue), FITC filter for FAM (green), and TRITC filter for compounds (red), respectively. The CLSM images of 0.5 h, 2 h and 4 h were obtained after incubation of the cells with condensates for different durations.

2.4. Endocytosis inhibition studies

Hela cells were first preincubated with 50 μM CPZ, 2.5 mM MβCD or 75 μM AM for 1h, then 1 mL of complexes in DMEM was added to each well. After 2 h incubation at 37 ºC, FAM positive cells were compared, determining which inhibitor played a critical role in decreasing the cellular uptake. Additionally, to study whether the cellular uptake of **TDM-B/DOPE** is energy-dependent, the polyplex was added to the cells, and cultured at 4 ºC for 2h.

2.5. GFP transfections in *vivo*.

Zebrafish embryos were provided by the China Zebrafish Resource Center. The **TDM-B**/DOPE-DNA complexes formed by 10 μg/mL eGFP DNA and 20 μM of **TDM-B**/DOPE in water for 30 min. Zebrafish embryos were incubated with 1 mL solutions containing the complexes for 5 h, then 1 mL fresh water was added and further incubated for 24 h. The fluorescence intensity of GFP was measured by confocal imaging, and Lipo2000 was used as a control. The relevant ethical protocols used for the *in vivo* study for zebrafish embryos were followed by the relevant laws. All experimental protocols were approved by the animal care committee of Beijing Normal University.

2.6. Gel Electrophoresis and Other Cellular Experiments.

Other experiments including agarose gel electrophoresis, ionic strength effect, releasing the compact DNA, EB displacement assay, cell toxicity, and cell transfection were conducted according to the procedures in reference. [14,19]

3. Results and discussion

3.1. Molecular design, synthesis and characterization

As depicted in Scheme 2, three 5,6-bis(4'-(diphenylamino)-[1,1'-biphenyl]-4-yl)pyrazine-2,3-diester modified [12]aneN$_3$ derivatives were originally designed and synthesized. In the molecules, the fluorophore structure were connected with triazole-[12]aneN$_3$ units through various length of alkyl chain. The AIE fluorophore **DCDPP-2TPA** (compound **1**) were prepared according to literature methods.[25,32] The conversion of cyano groups to carboxylic acids was achieved by hydrolysis in a strong base (6M KOH aq.) and further acidification to afford compounds **2**. Compound **2** were esterified with alcohols containing different length alkyl chain and an azido ending to give compounds **3a-3c**. The Propargyl [12]aneN$_3$ was

View Article Online
DOI: 10.1039/D0TB00391B

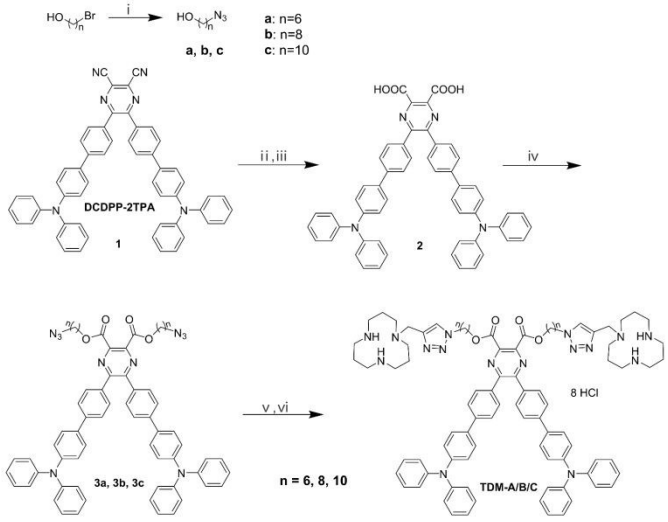

Scheme 2 Schematic route for **TDM-A, TDM-B** and **TDM-C**: (i) NaN_3, DMF, 65 ºC, 8 h; (ii) NaOH (6 M), Reflux, 24 h; (iii) HCl (2 M); (iv) NMM, EDCI, HOBT, TEA, r.t., 8 h; (v) Propargyl [12]aneN_3, CuBr, $CHCl_3$, r.t., 30 min; (vi) HCl-EtOAc, DCM, r.t., 2h.

prepared according to literature method we reported.[14] Through the highly efficient alkyne −azide click reactions catalyzed by Cu(I) and subsequent deprotections, the target compounds, **TDM-A/B/C**, were successfully synthesized as their hydrochloride salts. All the synthesized compounds were purified and further confirmed by ^{1}H NMR, ^{13}C NMR, FT-IR, and HR-MS (shown in the Supporting Information).

3.2. Solvatochromism and two-photon properties

The two triphenylamine groups (D, donor) were introduced into pyrazine-2,3-diester skeleton (A, acceptor) with phenyl unit to constitute the D-π-A conjugation. Thus, the photo-physics property of these compound is strongly dependent on the solvent polarity. Therefore, the absorption and photoluminescence (PL) spectra of **TDM-A/B/C** in solvents with different polarities were investigated, the results were summarized in Fig. 1 and Table S1. The maximum absorption wavelength of the three compounds were found to locate at ca. 400 nm in the various frequently used solvents, it can be attributed to the charge transfer (CT) transition absorption of the large conjugate system (Fig. S1). The wavelengths of the absorption maximum of **TDM-A/B/C** changed a few nanometers along the increase of the solvent polarity. On the contrary, the fuorescence spectra of the three compounds exhibited a very pronounced bathochromic-shift up to 383nm (from 547 nm to 748 nm). Simultaneously, the emission color changed from green to orange under 365 nm UV irradiation. The change of the fluorescent maximum with the solvent polarity parameter (ET(30)) were studied **(Fig. 2S)**,[22,33] the linear relationship was founded with the slopes to be 16.970, 17.660, and 17.445 for **TDM-A/B/C**, respectively. The above results indicate that the emission properties of **TDM** derivatives were strongly dependent on the solvent polarity, which could be likely ascribed to the TICT processes in these D-π-A structure molecules.[22] The absorption and fluorescent spectra of the three compounds are similar to those of **DCDPP-2TPA** in literatures,[33] but both the spectra showed a blue-shift relative to that of **DCDPP-2TPA**, which can be attributed to the weaker electro-withdrawing property of the ester groups in the three synthesized compounds when comparing with cyano groups in **DCDPP-2TPA**.

TDM-A/B/C with strong push −pull dipolar structures are characterized by interesting nonlinear optical properties, in particular, their two-photon absorption properties can be expected.[35,36] Thus, the two-photon excitation spectra of three compounds were measured in THF, and rhodamine B was used as the standards (Fig. S3 and Fig. S4). The emission signals were collected upon excitation from 720 to 800 (at 20 nm intervals). Impressively, the slopes of the linear relationships between laser power and the logarithm of fluorescence intensity were calculated to be 1.87, 1.88, and 1.82 (Fig. 2). In addition, they exhibit a maximum two-photon absorption cross-section (σ2P) of 109, 101, and 94 GM at 800 nm for **TDM-A/B/C**, respectively, which are beneficial to their biological application.

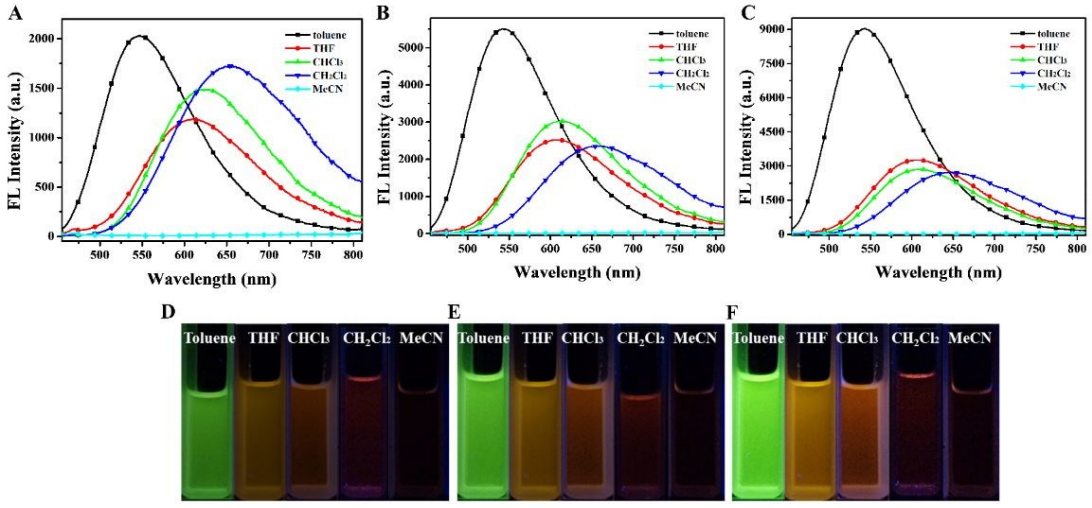

View Article Online
DOI: 10.1039/D0TB00321B

Fig. 1 (A–C) Fluorescence spectra of TDM-A (A), TDM-B (B) and TDM-C (C) in different solvents. (D–F) Images of TDM-A (D), TDM-B (E) and TDM-C (F) in different solvents taken under a UV 365 nm lamp. Concentrations: 10 μM, λex = 410 nm.

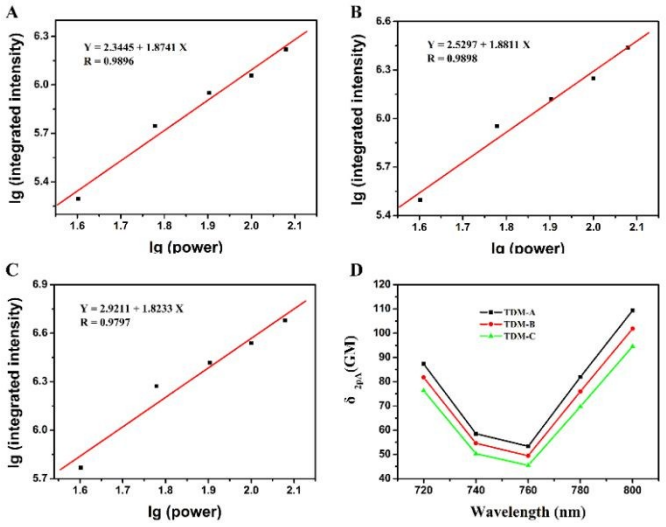

Fig. 2 Relationship between logarithm integrated intensity and logarithm laser power of **TDM-A** (A), **TDM-B** (B), and **TDM-C** (C) in THF. (D) Image of two-photon absorption (2PA) of the three **TDM** derivatives in THF solution. Concentration: 10 μM. Rhodamine B used as the standards.

TDM-A/B/C with strong push – pull dipolar structures are characterized by interesting nonlinear optical properties, in particular, their two-photon absorption properties can be expected.[35,36] Thus, the two-photon excitation spectra of three compounds were measured in THF, and rhodamine B was used as the standards (Fig. S3 and Fig. S4). The emission signals were collected upon excitation from 720 to 800 (at 20 nm intervals). Impressively, the slopes of the linear relationships between laser power and the logarithm of fluorescence intensity were calculated to be 1.87, 1.88, and 1.82 (Fig. 2). In addition, they exhibit a maximum two-photon absorption cross-section (σ2P) of 109, 101, and 94 GM at 800 nm for **TDM-A/B/C**, respectively, which are beneficial to their biological application.

3.3. Aggregation Induced Emission

To confirm whether the three compounds are AIE-active, their emission properties was studied in THF/water mixtures with different THF fractions (f_o) in volume (vol %) under an excitation of 410 nm. Unlike most reported typical AIEgens which are poor soluble in water, **TDM-A/B/C** are soluble in water, but they are virtually nonluminescent in aqueous solution. Their emission intensity is subjected to organic solvent content (f_o, THF fraction). As shown in Fig. 3 and Fig. S5, with increasing f_o in THF/water mixtures from 0 to 20%, the weak fluorescence of **TDM--A/B/C** (around 590 nm) enhanced gradually. When the THF fraction was increased to 30%, the maximal fluorescence intensities of **TDM--A/B/C** were decreased accompanied by a red-shift from 590 to 660 nm, which can be attributed to the change of the aggregation morphology.[18,37,38] The emission intensity of compounds further enhanced by the addition of THF fractions from 30% to 99% with a blue-shift from 650 to 610 nm. When the proportion of THF reached 99%, the maximum emission intensity of compounds **TDM-A/B/C** were 72, 81 and 108-fold higher than those in the pure water solution, respectively (Fig.

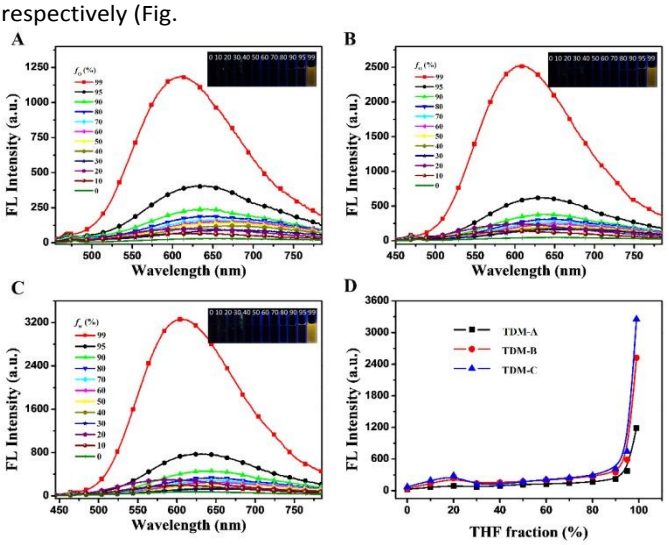

Fig. 3 Fluorescence spectra of **TDM-A** (A), **TDM-B** (B), and **TDM-C** (C) in water/THF mixtures with different THF fractions (f_o). Inset: Photographs of **TDM-A/B/C** in THF/water mixtures under the UV 365 nm lamp. (D) Plots of fluorescent intensities versus THF fractions for **TDM-A/B/C** in water/THF mixtures. Concentration: 10 μM; λ_{ex} = 410 nm.

S6). These are very typical phenomena for compounds bearing AIE characteristic.[37,39] Clearly, the aggregation-caused restriction rotational motions of molecular rotors (such as the phenyl rings of the triphenylamine moiety and pyrazine moiety) was responsible for the observed emission enhancement. These results demonstrated that **TDM-A/B/C** are typical AIE-active molecules. Fluorescent emission images displayed the immediate visualization fluorescent changes under 365 nm UV light.

Scanning electron microscopy (SEM) and dynamic light scattering (DLS) were further investigated to confirm the formation of aggregated nanoparticles with high THF fraction. The samples for the SEM measurement were prepared by adding THF to aqueous solution of the three compounds, and the well-assembled particles were formed after the THF/water mixtures stand for over 12 h, the regular nanoparticles were obtained with sizes of about 70 – 150 nm (Fig. S7). The results indicated the molecules undergo aggregation into a kind of particular arrangement in the THF/water mixtures.[40] The average diameters of the nanoparticles measured in solution by using DLS were 99, 141, and 194 nm for **TDM-A**, **TDM-B**, and **TDM-C**, respectively (Fig. S8), which were conformity with the SEM measurements.

3.4. Gel Electrophoresis Assays

In the course of gene transfection, it is very important to transform the negatively charged DNA into nanosized particles, which can reduce the electrostatic repulsion between DNA and cell surface. Furthermore, the formation of particles can also protect DNA to resist the degradation by nucleases in cytoplasm

View Article Online
DOI: 10.1039/D0TB00321B

or serum. Efficient condensation ability is the prerequisite for non-viral gene vectors. Thus, gel retardation assays were performed to test the DNA condensation ability of compound **TDM-A/B/C**. As shown in Fig. 4, the concentration for complete retardation with plasmid DNA (pDNA) by **TDM-A/B/C** were 10, 14, and 16 μM, respectively. The effective condensation ability can be ascribed to the electrostatic neutralization between the two triazole-[12]aneN$_3$ units and the negatively charged DNA phosphate groups, as well as the hydrophobic interactions of the two triphenylamine moiety and the aliphatic chain linkage. It was observed that **TDM-A** containing shorter alkyl chain linkage showed lower concentrations for the complete condensation. Furthermore, it was found that the complexes formed by mixing the three compounds with DOPE in a molar ratio of 1:2 further improved the condensation ability (Fig. 4D-F).[41] To be noticed, choosing the ratio of 1:2 of the three compounds with DOPE was derived from their good transfection performance (see 3.8).

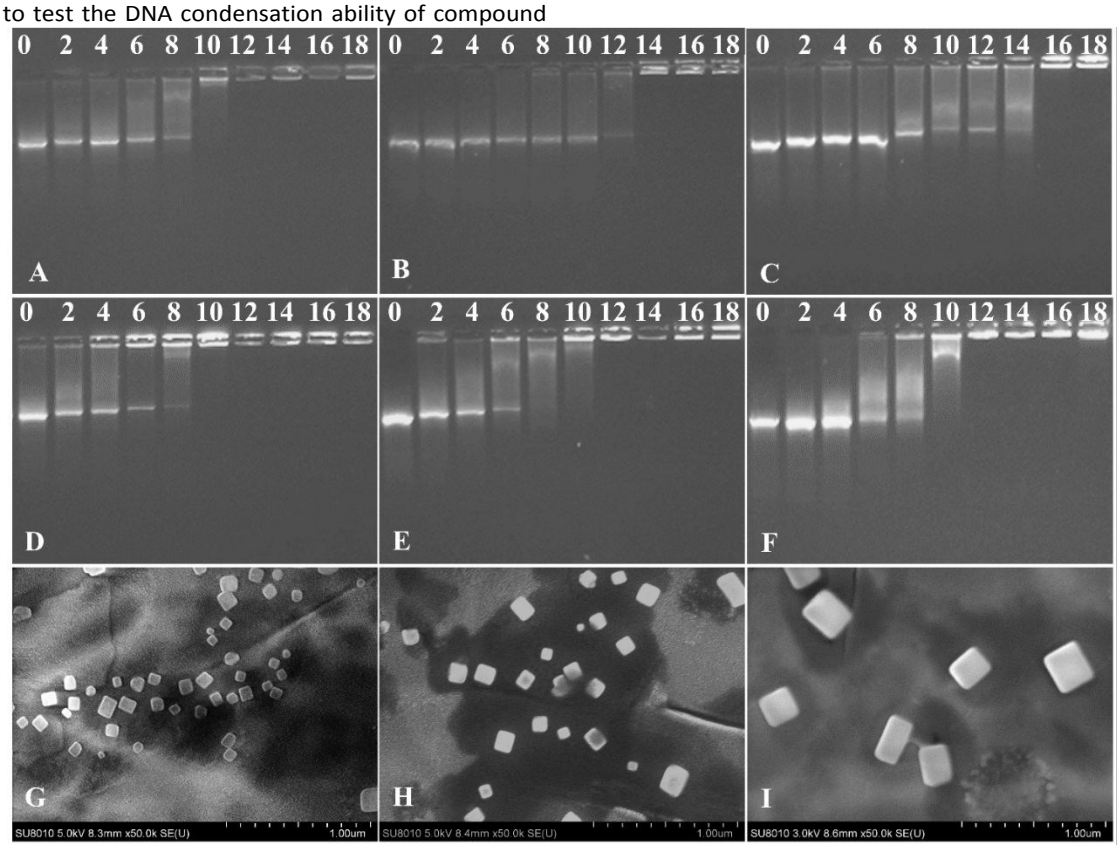

Fig. 4 Agarose gel electrophoresis assay of pUC18 DNA retardation induced by different concentrations (labeled on the top, μM) of **TDM-A/B/C** in the absence (A,C, E) and presence of DOPE (B, D, F) in 50 mM Trips-HCl (pH 7.4). The molar ratio of **TDM** derivatives/DOPE was 1:2, [DNA] = 9 μg/mL, 37 °C; SEM images of condensed pUC18 DNA (9 μg/mL) by **TDM-A/B/C** in Tris-HCl buffer (5 mM, pH 7.4): (A) **TDM-A**, 10 μM; (B) **TDM-B**, 14 μM; (C) **TDM-C**, 16 μM. Scale bars: 1 μm.

The condensing behaviors were further characterized by SEM and DLS measurements. As shown in Fig. 4, all of **TDM-A/B/C** effectively condensed DNA into the regular square nanoparticles with high dispersity and narrow size distributions, which were suitable for cell endocytosis and subsequent gene transfection.[18,41] The average sizes of these condensates obtained by DLS were 112, 103 and 111 nm (Fig. S9), respectively, which were similar to the SEM results. Moreover, the zeta potentials of the nanoparticles formed at the concentration for the complete DNA condensation were found to be 4.81, 8.92 and 6.18 mV, respectively (Fig. S10). The zeta potentials of the nanoparticles were lower than most report gene carriers, which can enhance the DNA stability in serum and decrease the cytotoxicity.[42]

At present, numerous tactics for triggering the dissociation of DNA from the condensing state have been developed. Herein, we investigated the pH effect or the presence of esterase in the release of the compacted DNA. As shown in Fig. S11, the condensed DNAs were mostly released after treated at pH5 for 1h, suggesting that the condensation process by the three compounds was reversible. Similarly, the addition of the lipase also resulted in the release of the condensed DNAs. The hydrolysis of ester bonds in the vectors should be responsible for the release of DNA and subsequent transfection studies.

3.5. Fluorescence response to ctDNA

The calf thymus DNA (ctDNA) is a natural dsDNA which has been widely used in the research of biochemical, chemical and medical science.[43-46] As shown in Fig. S12, the emission intensities of the three compounds gradually increased upon the addition of ctDNAs, their fluorescent intensities were almost linear-dependent to the ctDNA concentration with the correlation coefficients of 0.999, 0.972 and 0.988, respectively (Fig. S13). At the ctDNA concentration of 8 μg/mL, the fluorescence enhancements were 6.5-, 4- and 4-fold of the

View Article Online
DOI: 10.1039/D0TB00324B

original values for the three compounds (Table S2), indicating that the shorter linker of hydrophobic chain is beneficial to the interactions with DNA. Compared to the reported literature, the recognition of ctDNA by **TDM-A/B/C** showed a higher value of ($I/I_0 - 1$) at the same concentration, which may be caused by the multiple interactions between triazole[12]aneN$_3$

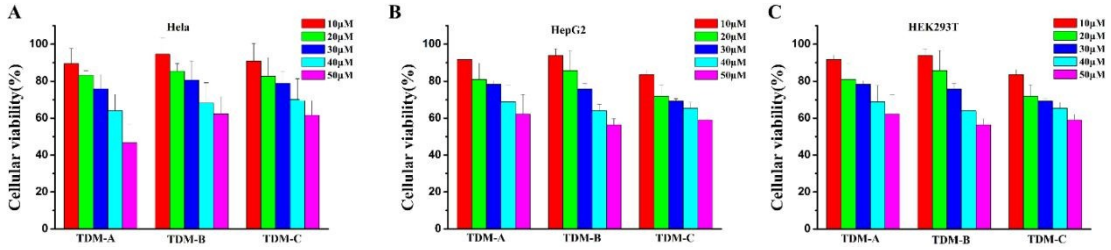

Fig. 5 Cytotoxicity of HeLa (A), HepG2 (B), and HEK293T (C) cells cultured with different concentrations of TDM-A, TDM-B and TDM-C.

moieties and ctDNAs.[19,21] The morphologies and sizes of the condensed nanoparticles were further characterized by SEM and DLS measurements. As shown in Fig. S14, SEM images clearly demonstrated that ctDNA was effectively condensed into regular nanoparticle by the three compounds. The mean diameters of the nanoparticles measured by DLS measurements (Fig. S6) are 79 nm (**TDM-A**), 135 nm (**TDM-B**), and 175 nm (**TDM-C**) (Fig. S15), which are consistent with those obtained by SEM.

3.6. EB Assay Experiments

The binding capabilities of **TDM-A/B/C** with DNAs were further evaluated by ethidium bromide (EB) exclusion assays.[47-49] As shown in Fig. S16, upon addition of **TDM-A/B/C** to the ctDNA-bounded EB solution, the fluorescent intensities of the solution were gradually diminished. The apparent binding constants (K_{app}) of **TDM-A/B/C** were deduced from the quenching plots (Fig. S17) to be 1.10×10^7, 0.99×10^7 and 0.86×10^7 M^{-1}, respectively. The result clearly proved the strong binding capabilities of these molecules interacted with ctDNA, the shorter alkyl linkage is slightly beneficial to the binding affinity. Compared to reported literatures, the high K_{app} value of the three compounds should be attributed to the synergetic contributions of the electrostatic interaction between the positively charged compounds and the negatively charged DNA phosphate backbones as well as the supramolecular stacking of **TDM** units with DNA through hydrophilic interactions, $\pi - \pi$ stacking, and hydrogen-bond interactions.[18,50]

3.7. Cytotoxicity

To assess the biocompatibility of the three compounds, we measured the cytotoxicity by 3-(4,5-dimethythiazol 2yl)-2,5-diphenyltetrazolium bromide (MTT) assay. As shown in Fig. 5, the cellular viabilities of HeLa, HpeG2 and HEK293T cells were investigated with increasing concentrations of the three compounds over 4 h, respectively. It can be seen that the increased cytotoxicity was observed with increasing feeding dosages, but all of the cells still maintained above 70% metabolic viabilities even at the concentrations up to 30 μM, which could be attributed to presence of the biocompatible triazole groups and the bio-reducible ester linkage in the molecules. In addition, the cytotoxicity of the three compounds were somewhat lower in Hela than in HpeG2 and HEK293T, and **TDM-B** showed lower toxicity in all cell lines. The above results indicated that the three compounds are suitable as safe carriers for delivering DNAs.

3.8. Cell Transfection

At first, quantitative evaluation of the transfection of the three compounds were determined by luciferase assay in the absence or presence of DOPE, which is a naturally occurring lipid frequently used as auxiliary lipid to elevate the endosomal escape, and effectively enhance the transfection efficiencies. It can be seen that the three compounds were able to transport pGL-3 plasmid successfully into HeLa, HpeG2 and HEK293T for genetic expression in the absence of DOPE. Clearly, the concentrations largely influenced the transfection efficiency, and the optimal concentrations were all located at 20-30 μM (Fig. S18). However, the overall transfection efficiencies were poor, the best transfection efficiencies of **TDM-A/B/C** in Hela cell lines were only 1.1, 12 and 0.3% compared with those of the commercial transfection reagent Lipo2000.

Then, the transfections of the liposome formed by **TDM-A/B/C** and DOPE were explored. The cell transfections in Hela cell lines with the liposomes of the three compounds and DOPE were investigated in detail (at different concentrations and different molar ratios). It was found that the liposome formed by mixing the three compounds with DOPE in a molar ratio of 1:2 afforded the best transfection efficiency, and the transfection efficiencies of **TDM-B**/DOPE was 156% of that achieved by Lipo2000 (Fig. 6). Results from the transfection assays in Hela cells clearly demonstrated that the three compounds hold great promise as non-viral gene carriers, and **TDM-B** showed the best transfection efficiencies among the three compounds.

Under optimal conditions, transfection assays mediated were also carried out in HepG2 and HEK293T cells. As shown in Fig. 7, among the three types of cancer cells tested, the best transfection efficiencies are observed with the HeLa cell lines, then the HEK293T cell lines, followed by the HepG2 cell lines. The optimal transfection efficiencies compared with Lipo2000 were summarized in Table S3. The transfection efficiencies of **TDM-B**/DOPE in HepG2 and HEK293T cells were 87, and 130% that of Lipo2000, respectively. The above results indicated that the three compounds with rigid **TDM** frameworks can act as generally applicable non-viral gene vectors.

The visual transfections of the compounds were obtained through the expression of pEGFP-N1 reporter gene in the Hela

View Article Online
DOI: 10.1039/D0TB00324B

cell lines. The results indicated that the GFP genes were successfully delivered to the expression of GFP by the three compounds (Fig. 8 and Fig. S19). It can be seen that **TDM-B** still showed higher TEs than **TDM-A** and **TDM-C**. Noteworthy, the transfection efficiency of **TDM-B** /DOPE was much better than

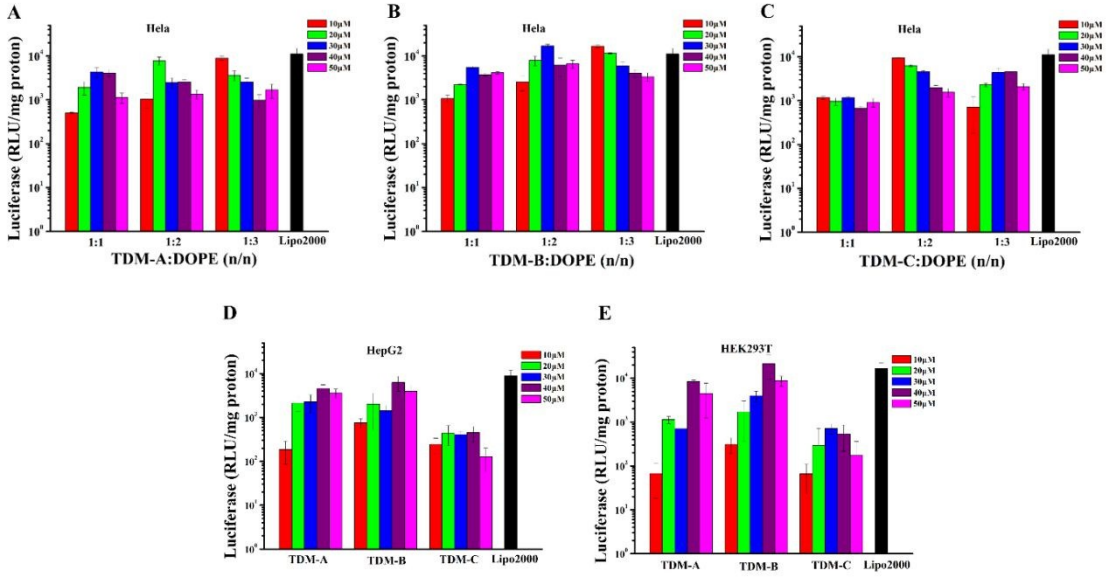

Fig. 6 Luciferase expressions transfected by liposomes TDM-A/DOPE(A), TDM-B/DOPE(B), TDM-A/DOPE(C), with molar ratios of 1:1-1:3 at varying concentrations in Hela cell lines. Luciferase expressions transfected by liposomes TDM-A/DOPE, TDM-B/DOPE, TDM-A/DOPE, with molar ratios of 1:2 in HepG2 cell lines (D) and HEK293T cell lines(E). [pGL-3] = 10 μg/mL.

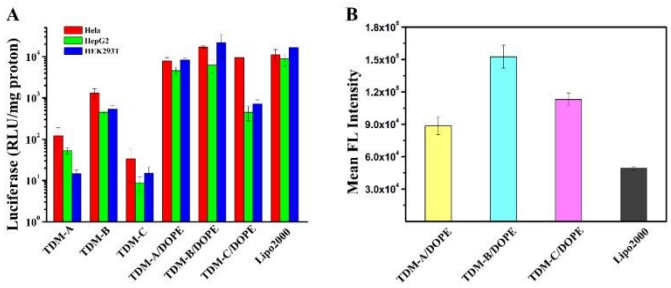

Fig. 7 Result histogram of luciferase expressions mediated by **TDM-A/B/C** in the absence and presence of DOPE under respective optimal conditions with Lipo2000 as control. [pGL-3] = 10 μg/mL (A). GFP expression for **TDM-A/B/C** in the presence of DOPE in Hela cells under respective optimal conditions with Lipo2000 as control (B). Concentrations for the three compounds were 20 μM (**TDM-A** and **TDM-B**) and 30 μM (**TDM-C**); [pEGFP-N1] = 10 μg/mL.

The visual transfections of the compounds were obtained through the expression of pEGFP-N1 reporter gene in the Hela cell lines. The results indicated that the GFP genes were successfully delivered to the expression of GFP by the three compounds (Fig. 8 and Fig. S19). It can be seen that **TDM-B** still showed higher TEs than **TDM-A** and **TDM-C**. Noteworthy, the transfection efficiency of **TDM-B** /DOPE was much better than that acquired by Lipo2000. We also quantitatively evaluate the GFP genes transfection efficiency of these compounds and their liposomes by flow cytometry. Under optimal conditions, the transfection efficiencies of **TDM-A**/DOPE, **TDM-B**/DOPE and **TDM-C**/DOPE were 1.8, 3.1 and 2.3 times of that by Lipo2000, respectively. Simultaneously, the weak red fluorescence in the red channel were produced by the AIE phenomenon after the release of DNA from the liposomes.

Based on the transfection results, several points can be concluded. First, the liposomes of the three compounds with DOPE efficiently delivered plasmid DNAs (pGL-3 and pEGFP-N1 reporter genes) into HepG2, HEK293T and Hela cell lines, the

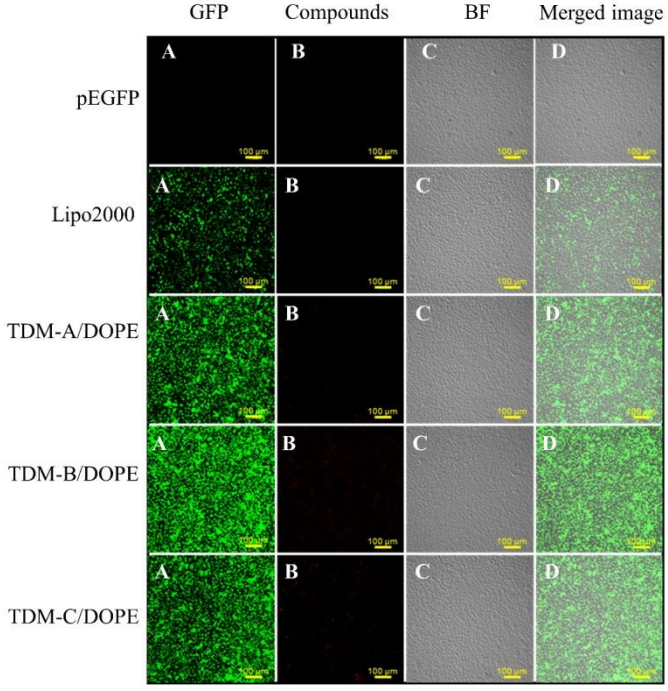

Fig. 8 Fluorescence microscope images (10×) of pEGFP-transfected in Hela cells. GFP was observed with FITC filter (A); The inherent red fluorescence of **TDM-A/B/C** were observed with the TRITC filter (B); Bright field (C); Merge of A, B, C. GFP (D). Lipo2000 and naked pEGFP-N1 were used as control. Concentration = 20 μM; [pEGFP-N1] = 10 μg/mL, scale bar: 100 μm.

View Article Online DOI: 10.1039/D0TB00231B

transfection efficiencies in HeLa cells were much higher than those in A549 and HepG2 cells. Considering that different cell types have distinct pathways, the different transfection performance of the three compounds among various cell lines is reasonable. Secondly, the best transfection efficiencies obtained for **TDM-B**/DOPE in a molar ratio of 1:2 were significantly higher than that of Lipo2000, which came up to

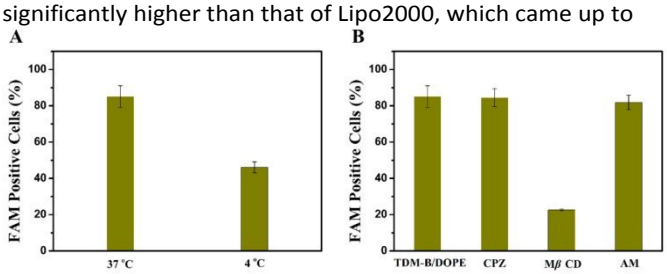

Fig. 9 Cellular uptake of **TDM-B**/DOPE-DNA complexes incubated at 37 and 4 °C (A). The internalization of **TDM-B**/DOPE-DNA complexes in the presence of different inhibitors (B). [**TDM-B**] = 20 μM, [pEGFP-N1] = 10 μg/mL.

1.54 times for luciferase expressions and 3.1 times GFP expressions, respectively. Thirdly, it clearly demonstrated that the transfection efficiencies of **TDM-A/B/C** are closely related to the alkyl length of the linkage between the TDM unit and the triazole-[12]aneN$_3$, the eight carbon alkyl linkage exhibited good transfection efficiencies.

3.9. Cellular uptake mechanism study

The vectors' performance is closely related to the intracellular kinetics, the detailed polyplex cellular uptake level, internalization pathway, and DNA release need further definition. As a gene delivery system, the internalization pathway of **TDM-B/**DOPE with DNA is a basic parameter to be analyzed. To confirm which endocytosis is decisive in the cellular uptake, the active transport process was investigated with a temperature change. In consequence, the cellular uptake efficiency decreased to 46% at 4 °C compared to that of 85% at 37 °C (Fig. 9 and Fig. S20), which clearly indicated that the cellular uptake of **TDM-B/**DOPE was greatly through the energy-dependent endocytosis. Chemical inhibitors such as chlorpromazine (CPZ), amiloride hydrochloride (AM), and methyl-β-cyclodextrin (M*β*CD) may inhibit the cellular uptake pathways of clathrin-mediated endocytosis (CME), micropinocytosis, and clathrin-independent endocytosis (CIE), respectively.[42,51,52] It was found that the cellular uptake efficacy decreased slightly to 84% and 81% in the presence of CPZ and AM, respectively (Fig. 9 and Fig. S21). Sharply differently, the cellular uptake efficacy was reduced to 5% with M*β*CD preincubation. Accordingly, we can firmly believe that the ultrahigh cellular uptake efficacy of **TDM-B/**DOPE formulated with DNA mainly proceed via a CIE pathway.

3.10. Single Photon Fluorescent Tracing the Delivery of DNA

Inspired by the performance of the transfection and its optical property, TDM-B/DOPE was singled out as representative for tracing the gene delivery process by single-photon fluorescence microscopy. The condensates of TDM-B/DOPE with FAM-labeled DNA were incubated in vitro with Hela cell lines for varying times. The TDM-B/DOPE and FAM-labeled DNA were visualized through the red channel and green channel, respectively. In order to locate the DNA complex, the nucleus was stained by Hoechst 33342, a nucleus-specific blue fluorescent dye. As shown in Fig. 10, only a small fraction of blue-emission condensates entered into the cells at 0.5 h, and the condensates mainly accumulated near the cell membrane. After 1 h of incubation, more condensates transferred into the

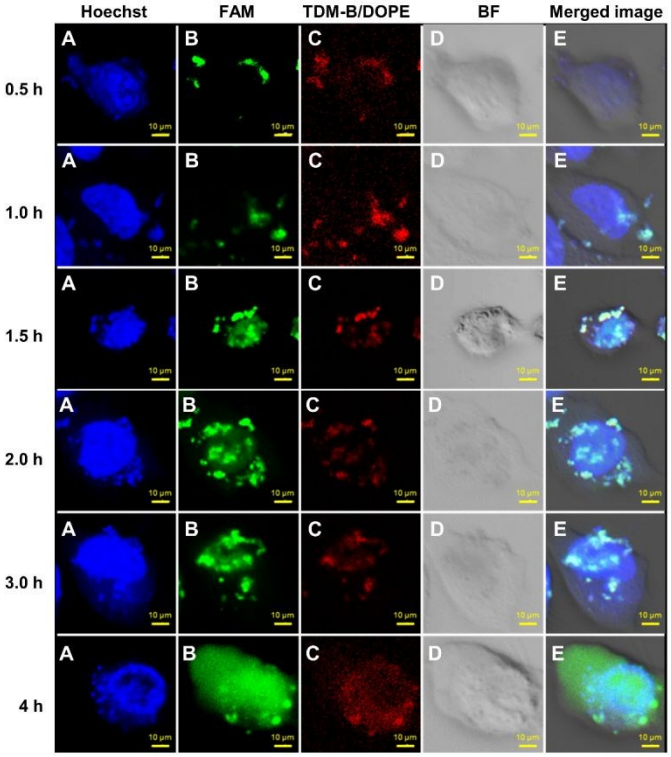

Fig. 10 CLSM images (60×) of **TDM-B**/DOPE (1:2) at 0.5, 1, 1.5, 2, 3, and 4 h after delivery into Hela cells. The nucleus (blue channel) (A). The FAM-labeled DNA (green channel) (B). **TDM-B**/DOPE (red channel) (C). Bright field (D) and Merge of A, B, C (E). [**TDM-B**] = 20 μM, [FAM-DNA] = 10 μg/mL, scale bar: 10 μm.

cells, and the majority of them were found to locate in cytoplasm. It is noteworthy that weak fluorescence of the nucleus revealed that some condensates had already translocated into the nucleus. Upon further incubation for 2 and 4 h, the green fluorescence intensity of the nucleus became stronger, proving more condensates entered into the nucleus. These results demonstrate that this unique gene vector can indeed enter into the nucleus together with DNAs rapidly. Furthermore, this delivery behavior could effectively prevent degrading the released DNA in cytoplasm from the DNase, which might be responsible for the decent transfections shown by the **TDM-B/**DOPE liposome. To be noticed, some spots can be seen in cells under Hoechst staining, which can be attributed to the DNA complex condensates remained.

3.11. Two-Photon Fluorescent Tracing of the Delivery of DNA

Based on the excellent two-photon characteristics of the **TDM** derivatives, the DNA delivery process with the liposome **TDM-B**/DOPE were further explored under an excitation of 800 nm. Parallel results were shown in Fig. 11, the DNA delivery process were observed more clearly through two-photon fluorescence

microscopy. The liposome-loaded DNA was efficiently delivered into the cytoplasm by endocytosis in two hours, and a portion of condensates had already got into the nucleus. As the incubation time was increased to 4 h, more and more condensates gradually transferred into the nucleus. When the incubation lasted to 6 hours, it was clearly observed that most of the DNA were released from the liposomes and the vector were discarded into cytoplasm reassembled into micelles (white arrows) with weak red-emission. Upon further incubation for 12 hours, the red fluorescence of the vector was nearly completely separated from FAM-DNA, and the vector was excreted in the metabolic process. Considering the spatiotemporal transition of the intracellular fluorescence and the distribution, the fate of the internalized condensates can be easily monitored, which would contribute to the further comprehension of the transfection mechanism.

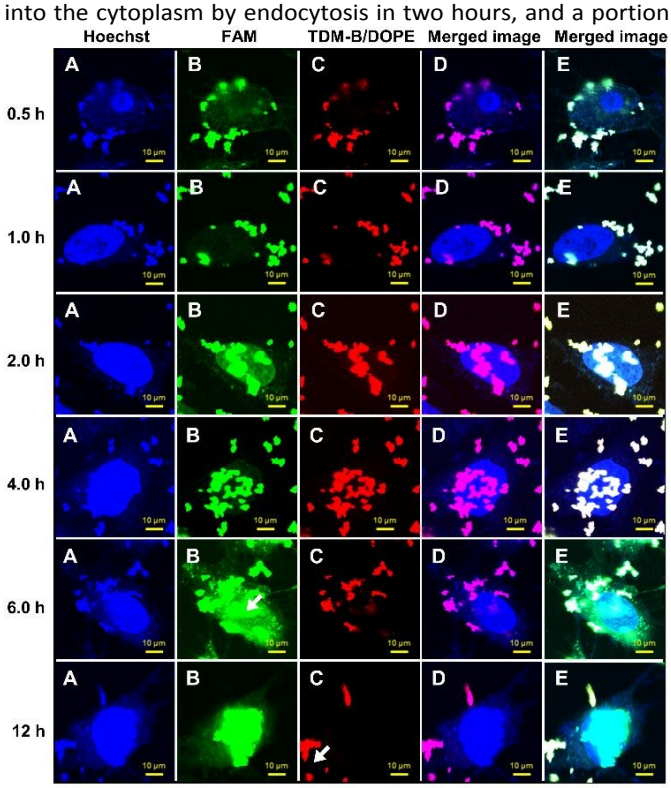

Fig. 11 CLSM images (60×) of **TDM-B**/DOPE (1:2) at 0.5, 1, 2, 4, 6, and 12 h after delivery into Hela cells. The nucleus (blue channel) (A). The FAM-labeled DNA (green channel) (B). **TDM-B**/DOPE (red channel) (C). Merge of a and c (D). Merge of A, B, C (E). [**TDM-B**] = 20 μM, [FAM-DNA] = 10 μg/mL, λ_{ex} = 800 nm, scale bar: 10 μm.

3.12. GFP transfections *in Vivo*

Encouraged by the transfection results *in vitro*, the gene expressions experiments of **TDM-B/**DOPE *in vivo* were further studied by introducing the reporter gene EGFP-DNA in developing zebrafish embryos. Zebrafish is an ideal vertebrate model for biological in vivo imaging, owing to the exceptionally high optical clarity in embryonic and larval stages.[53] After treatment of the **TDM**-B/DOPE-DNA complexes into zebrafish, the fluorescence intensity of GFP was measured by confocal imaging, and Lipo2000 was used as a control (Fig. 12). It was found that the GFP gene expression level of **TDM-B/**DOPE was about 2-fold higher than that of Lipo2000 in zebrafish embryos. The effectiveness to enhance the transfection effect of GPF in

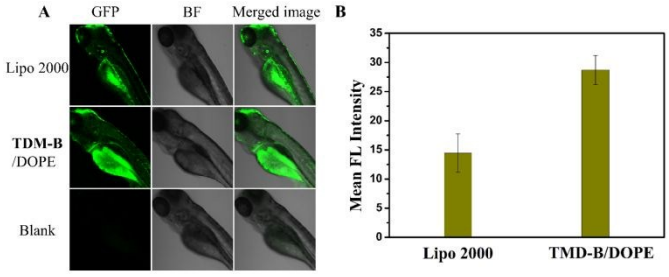

Fig. 12 *In vivo* GFP transfection: confocal image (A) and fluorescence intensity (B) of GFP expression in zebrafish embryos. [**TDM-B**/DOPE] = 20 μM, [EGFP-DNA] = 10 μg/mL; Lipo2000 was used as a control.

physiological environment proved that **TDM-B/**DOPE was an effective non-viral gene vector in this *in vivo* work.

4. Conclusions

In this study, the near-infrared fluorescent unit with the aggregation-induced emission and two photon absorption properties triphenylamine-pyrazine with DNA condensing moieties triazole-[12]aneN3 through the different length alkyl ester linkage to afford three new non-viral gene vectors, TDM-A/B/C. The three compounds showed strong AIE features upon the addition of THF as a poor solvent with the fluorescent emission enhancements to be 72, 81, and 108-fold higher than those in pure water solutions, respectively. The largest stokes shift of the three compounds up to 383 nm and the large 2PA cross section up to 101 GM for TDM-B were achieved. Gel electrophoresis demonstrated that TDM-A/B/C were able to completely retard the movement of plasmid DNA at the concentration of 10, 14, and 16 μM, respectively. Simultaneously, under esterase and acidic environment, the condensed DNA were able to be reversely released due to the hydrolysis of ester bonds in the three compounds. From SEM study, the compounds themselves, their liposome and their lipoplexes can be assembled into regular cubic nanoparticles, the sizes of the lipoplexes nanoparticles were in the range of 100-200 nm, which were further confirmed by DLS measurements, and the lipoplexes showed zeta potential to be 4-9 mV for three compounds. The cytotoxicity of the three compounds were also good for the gene transfection. Among the three compounds, TDM-B showed the best transfection efficiencies, and the expression of luciferase and GFP was 146% and 310% of those achieved by Lipo2000 in Hela cells. The One/two-photon fluorescence microscopic image with TDM-B clearly revealed the transfection process of DNA, the DNA were efficiently delivered into the nucleus in 4 hours. Moreover, TDM-B/DOPE were successfully implemented gene transfection in zebrafish embryos, and the EGFP gene expression level was about 2-fold higher than that of Lipo2000. The work also demonstrated that the length of aliphatic chain linkage affected the DNA delivery and transfection, the chain with eight carbon

atoms gave the best transfection results. This study provides information regarding improvements of real-time tracking during gene delivery, transfection and the rational design of multifunctional non-viral vectors.

Conflicts of interest

There are no conflicts to declare.

Acknowledgements

This study was supported by the National Natural Science Foundation of China (21372032, and 21778012), and the Drug Innovation Major Project (2018ZX09711001002-005). L.H. thanks the government of the Guangxi Autonomous Region for being the fifth batch of distinguished experts.

References

1 H. Yin, R. L. Kanasty, A. A. Eltoukhy, A. J. Vegas, J. R. Dorkin, D. G. Anderson, *Nat. Rev. Genet.*, 2014, **15**, 541-555.
2 H. M. Leung, M. S. Chan, L. S. Liu, S. W. Wong, T. W. Lo, C.-H. Lau, C. Tin, P. K. Lo, *ACS Sustainable Chem. Eng.*, 2018, **6**, 9671-9681.
3 C. E. Dunbar, K. A. High, J. K. Joung, D. B. Kohn, K. Ozawa, M. Sadelain, *Science*, 2018, **359**, eaan4672.
4 L. H. Wang, D. C. Wu, H. X. Xu, Y. Z. You, *Angew. Chem. Int. Ed. Engl.*, 2016, **55**, 755-759.
5 S. D. Li, L. Huang, *Gene Ther.*, 2006, **13**, 1313-1319.
6 L. S. Young, P. F. Searle, D. Onion, V. Mautner, *J. Pathol.*, 2006, **208**, 299-318.
7 J. F. Wright, *Gene Ther.*, 2008, **15**, 840-848.
8 S. Bhattacharya, A. Bajaj, *Chem. Commun.*, 2009, 4632-4656.
9 C. E. Thomas, A. Ehrhardt, M. A. Kay, *Nat. Rev. Genet.*, 2003, **4**, 346-358.
10 Q. Huang, S. Li, Y.-F. Ding, H. Yin, L.-H. Wang and R. Wang, *Biomater. Sci.*, 2018, **6**, 1031-1039.
11 W. C. Geng, Q. Huang, Z. Xu, R. Wang and D. S. Guo, *Theranostics*, 2019, **9**, 3094-3106.
12 M. A. Mintzer, E. E. Simanek, *Chem. Rev.*, 2009, **109**, 259-302.
13 M. Munoz-Ubeda, S. K. Misra, A. L. Barran-Berdon, C. Aicart-Ramos, M. B. Sierra, J. Biswas, P. Kondaiah, E. Junquera, S. Bhattacharya, E. Aicart, *J. Am. Chem. Soc.*, 2011, **133**, 18014-18017.
14 A. X. Ding, Z. L. Tan, Y. D. Shi, L. Song, B. Gong, Z. L. Lu, *ACS Appl. Mater. Interfaces*, 2017, **9**, 11546-11556.
15 C. H. Jones, C. K. Chen, A. Ravikrishnan, S. Rane, B. A. Pfeifer, *Mol. Pharm.*, 2013, **10**, 4082-4098.
16 X. Guo, L. Huang, *Acc. Chem. Res.*, 2012, **45**, 971-979.
17 M. You, G. Zhu, T. Chen, M. J. Donovan, W. Tan, *J. Am. Chem. Soc.*, 2015, **137**, 667-674.
18 A. X. Ding, Q. Tang, Y. G. Gao, Y. D. Shi, A. Uzair, Z. L. Lu, *ACS Appl. Mater. Interfaces*, 2016, **8**, 14367-14378.
19 Y.-G. Gao, Q. Tang, Y.-D. Shi, Y. Zhang, R. Wang, Z.-L. Lu, *RSC Adv.*, 2016, **6**, 50053-50060.
20 A. I. Dragan, E. S. Bishop, R. J. Strouse, J. R. Casas-Finet, M. A. Schenerman, C. D. Geddes, *Chem. Phys. Lett.*, 2009, **480**, 296-299.
21 P. Yue, Y. Zhang, Z. F. Guo, A. C. Cao, Z. L. Lu, Y. G. Zhai, *Org. Biomol. Chem.*, 2015, **13**, 4494-4505.
22 M. Jiang, X. Gu, J. W. Y. Lam, Y. Zhang, R. T. K. Kwok, K. S. Wong, B. Z. Tang, *Chemical science*, 2017, **8**, 5440-5446.
23 M. Gao, H. Su, S. Li, Y. Lin, X. Ling, A. Qin, B. Z. Tang, *Chem. Commun.*, 2017, **53**, 921-924.
24 Z. Zheng, T. Zhang, H. Liu, Y. Chen, R. T. K. Kwok, C. Ma, P. Zhang, H. H. Y. Sung, I. D. Williams, J. W. Y. Lam, K. S. Wong, B. Z. Tang, *ACS Nano*, 2018, **12**, 8145-8159.
25 Y. Wang, M. Chen, N. Alifu, S. Li, W. Qin, A. Qin, B. Z. Tang, J. Qian, *ACS Nano*, 2017, **11**, 10452-10461.
26 M. X. Liu, L. L. Ma, X. Y. Liu, J. Y. Liu, Z. L. Lu, R. Liu, L. He, *ACS Appl. Mater. Interfaces*, 2019, **11**, 42975-42987.
27 S. S. Le Corre, N. Belmadi, M. Berchel, T. Le Gall, J. P. Haelters, P. Lehn, T. Montier, P. A. Jaffres, *Org. Biomol. Chem.*, 2015, **13**, 1122-1132.
28 E. Ojeda, G. Puras, M. Agirre, J. Zarate, S. Grijalvo, R. Pons, R. Eritja, G. Martinez-Navarrete, C. Soto-Sanchez, E. Fernandez, J. L. Pedraz, *Org. Biomol. Chem.*, 2015, **13**, 1068-1081.
29 B. Q. Liu, W. J. Yi, J. Zhang, Q. Liu, Y. H. Liu, S. D. Fan, X. Q. Yu, *Org. Biomol. Chem.*, 2014, **12**, 3484-3492.
30 X. Gao, L. Huang, *Gene Ther.*, 1995, **2**, 710-722.
31 D. Zhi, S. Zhang, B. Wang, Y. Zhao, B. Yang, S. Yu, *Bioconjug. Chem.*, 2010, **21**, 563-577.
32 S. Y. Chen, X. J. Xu, Y. Q. Liu, G. Yu, X. B. Sun, W. F. Qiu, Y. Q. Ma, D. B. Zhu, *Adv. Funct. Mater.*, 2005, **15**, 1541-1546.
33 C. Reichardt, *Chem. Rev.*, 1994, **94**, 2319-2358.
34 B. Gao, Q. Zhou, Y. Geng, Y. Cheng, D. Ma, Z. Xie, L. Wang, F. Wang, *Mater. Chem. Phys.*, 2006, **99**, 247-252.
35 B. K. Agrawalla, H. W. Lee, W. H. Phue, A. Raju, J. J. Kim, H. M. Kim, N. Y. Kang, Y. T. Chang, *J. Am. Chem. Soc.*, 2017, **139**, 3480-3487.
36 Y. L. Pak, S. J. Park, Q. Xu, H. M. Kim, J. Yoon, *Anal. Chem.*, 2018, **90**, 9510-9514.
37 Y. Hong, J. W. Lam, B. Z. Tang, *Chem. Commun.*, 2009, 4332-4353.
38 Z. Zhao, S. Chen, X. Shen, F. Mahtab, Y. Yu, P. Lu, J. W. Lam, H. S. Kwok, B. Z. Tang, *Chem. Commun.*, 2010, **46**, 686-688.
39 Y. Hong, J. W. Lam. B. Z. Tang, *Chem. Soc. Rev.*, 2011, **40**, 5361-5388.
40 Y. Cao, M. Yang, Y. Wang, H. Zhou, J. Zheng, X. Zhang, J. Wu, Y. Tian, Z. Wu, *J. Mater. Chem. C*, 2014, **2**, 3686-3694.
41 Y. G. Gao, Y. D. Shi, Y. Zhang, J. Hu, Z. L. Lu, L. He, *Chem. Commun.*, 2015, **51**, 16695-16698.
42 S. Liu, D. Zhou, J. Yang, H. Zhou, J. Chen, T. Guo, *J. Am. Chem. Soc.*, 2017, **139**, 5102-5109.
43 A. L. Barran-Berdon, B. Yelamos, L. Garcia-Rio, O. Domenech, E. Aicart, E. Junquera, *ACS Appl. Mater. Interfaces*, 2015, **7**, 14404-14414.
44 M. Lan, W. Liu, Y. Wang, J. Ge, J. Wu, H. Zhang, J. Chen, W. Zhang, P. Wang, *ACS Appl. Mater. Interfaces*, 2013, **5**, 2283-2288.
45 G. Zhang, Y. Zhang, Y. Zhang, Y. Li, *Sensors and Actuators B: Chemical*, 2013, **182**, 453-460.
46 W. Zhu, C. Xuan, G. Liu, Z. Chen and W. Wang, *Sensors and Actuators B: Chemical*, 2015, **220**, 302-308.
47 B. Sun, J. X. Guan, L. Xu, B. L. Yu, L. Jiang, J. F. Kou, L. Wang, X. D. Ding, H. Chao and L. N. Ji, *Inorg. Chem.*, 2009, **48**, 4637-4639.
48 B. C. Baguley and M. Le Bret, *Biochemistry*, 1984, **23**, 937-943.
49 J. T. Wang, Q. Xia, X. H. Zheng, H. Y. Chen, H. Chao, Z. W. Mao, L. N. Ji, *Dalton Trans.*, 2010, **39**, 2128-2136.
50 K. X. Zhang, A. X. Ding, Z. L. Tan, Y. D. Shi, Z. L. Lu, L. He, *J. Photoch. Photobio. A*, 2018, **355**, 338-349.
51 S. D. Conner, S. L. Schmid, *Nature*, 2003, **422**, 37-44.
52 K. S. Lim, D. Y. Lee, G. M. Valencia, Y.-W. Won, D. A. Bull, *Adv. Funct. Mater.*, 2015, **25**, 5445-5451.
53 D. Wang, H. Su, R. T. K. Kwok, G. Shan, A. C. S. Leung, M. M. S. Lee, H. H. Y. Sung, I. D. Williams, J. W. Y. Lam and B. Z. Tang, *Adv. Funct. Mater.*, 2017, **27**, 1704039.

View Article Online
DOI: 10.1039/D0TB00321B

Graphical Abstract

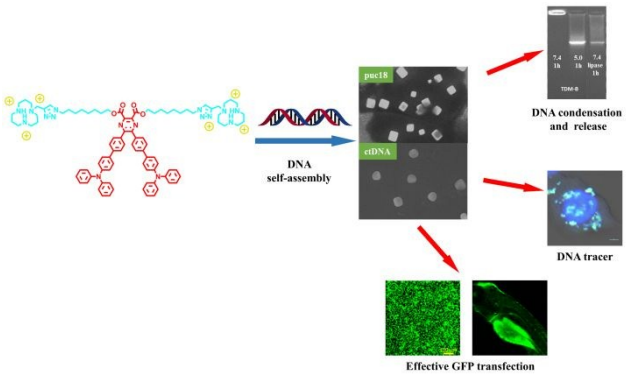

[12]aneN_3 Modified triphenylamine-pyrazines as non-viral gene vectors with AIE and two-photon imaging properties.